Point bar deposits in narrow sharp bends
Barres de méandres en canal étroit à forte courbure

S. KAWAI
Associate Professor of Civil Engineering, Maizuru College of Technology, Maizuru, Kyoto 625, Japan

P.Y. JULIEN
Professor of Civil Engineering, Engineering Research Center, Colorado State University, Fort Collins, CO 80523, USA

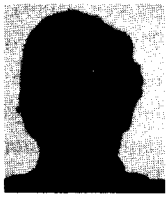

ABSTRACT
Meandering channels typically deposit sediments near their inner bank to form point bars. Laboratory experiments with narrow sharp bends show that under identical flow conditions the configuration of point bars depends on particle size. Explanation to this grain-size effect is found in a three-dimensional particle stability. Despite favorable secondary currents, coarse grains tend to move toward the thalweg and coarse-grained point bar deposits are eroded as the side-slope angle approaches the angle of repose of the bed material. Calculated results coincide with experimental observations. Point bars are considerably smaller for coarse-sand deposits than fine sands.

RÉSUMÉ
Les cours d'eau à méandres déposent leurs alluvions près de la berge convexe pour former des barres de méandres. Les expériences de laboratoire en canal étroit à forte courbure montrent qu'en présence d'écoulements identiques, la configuration des dépôts dépend de la taille des sédiments. Une analyse tridimensionnelle de la stabilité des sédiments sur une barre de méandres explique la formation des dépôts. En dépit d'écoulements secondaires favorables, les sédiments grossiers se déplacent vers le thalweg et les barres de méandres en sédiments grossiers s'amenuisent lorsque la pente des dépôts approche l'angle de frottement interne des alluvions. Les résultats calculés coïncident avec les observations expérimentales: la dimension des barres de méandres varie en raison inverse de la taille des sédiments.

40 Word summary
Under identical hydraulic conditions, point bar configuration depends on grain size. A three-dimensional particle stability analysis confirms experimental results that coarse-grained point bars are smaller than fine-grained deposits. In narrow sharp bends, deposits are limited at steep side-slope angles.

Key words
Point bars, river bends, particle stability, secondary flow, sediment deposits.

1 Introduction

Bed deformation in river bends is important to determine the rate of lateral migration of natural meandering channels. With the expansion of living communities on river banks, engineers are concerned with the prevention of lateral migration. Bank protection structures are designed to ensure river bank stability.

The deformation of river bends has been studied for centuries, and it is widely known that alluvial rivers erode their outer bank while sediment is deposited near their inner bank to form point bars.

Revision received January 18, 1996. Open for discussion till October 31, 1996.

Early field and laboratory investigations were carried out by Engels, Leliavsky, Fargue and Friedkin. Subsequent developments were proposed by Rozovskii (1957), Muramoto et al. (1968), Yen (1970), Kikkawa et al. (1976), Zimmermann and Kennedy (1978), Koch and Flokstra (1980), Odgaard (1981), Ikeda (1982), Parker (1984), Struiksma et al. (1985), and Talmon et al. (1995) among many others. Recent reviews can be found under the editorship of Elliott (1984), Ikeda and Parker (1989), and Shen (1990).

The interest for this study arises from the authors' experimental observations of point bar deposits in small-scale laboratory models of meander bends. The vertical scale of hydraulic models in the laboratory is generally distorted (amplified in comparison to the horizontal scale) in order to maintain a sufficient flow depth the ease laboratory measurements and avoid surface tension effects. Distorted river models typically have a smaller width/depth ratio than the corresponding prototype. Besides perturbing turbulent mixing scales in the horizontal and vertical directions, the side-slope angle of distorted models is considerably increased.

Experiments were carried out in a curved laboratory channel with fine sand transported under steady flow discharge. A widespread point bar forms near the inner bank of the channel bend. When the experiment is repeated with coarse sand in the same channel, under identical flow conditions, only a short point bar is observed. The experimental fact that point bar configurations depend on grain sizes under identical flow conditions triggered the search for a physical explanation.

The objective of this study is to explain the difference in point bar configuration from a particle stability analysis. The bed deformation in a bend is investigated theoretically and experimentally with attention focused on the point bar near the inner bank of a narrow meandering laboratory channel. First, a three-dimensional particle stability analysis is presented to determine the direction angle of sand particles in a river bend. The experimental study is then described, showing the different point bar configurations observed with coarse and fine sands. Finally, the experimental results are explained in view of the particle stability analysis.

2 Particle stability analysis

2.1 *Method*

The stability of a particle subjected to three-dimensional hydrodynamic forces on a side slope proposed by Julien (1995) is briefly explained herein as it applies to a typical point bar configuration. Figure 1 illustrates the forces acting on a non-cohesive particle p located on a point bar at a side slope angle θ_1, and a downstream bed slope angle θ_0. Geometrically, one defines $a_\theta = \sqrt{\cos^2\theta_1 - \sin^2\theta_0}$ and $\tan\theta = \sin\theta_0/\sin\theta_1$ from the downstream angle θ_0 and the side slope angle θ_1. One recognizes the lift force F_L, the drag force F_D, the buoyancy force F_B, and the weight of the particle F_W. As long as the water surface slope angle in the downstream direction is small, the near-vertical buoyancy force can be subtracted from the weight of the particle to give the submerged weight of the particle $F_S = F_W - F_B$. The lift force is defined as the fluid force normal to the embankment plane whereas the drag force is acting along the plane in the same direction as the velocity field surrounding the particle.

The submerged weight exerts one sideslope component $F_S \sin\theta_1$, one downstream component $F_S \sin\theta_0$, and a component normal to the plane $F_S a_\theta$. The streamline deviates from the downstream direction at an angle λ defined positive downward along the embankment plane. On a point bar, the angle λ is negative, and can be calculated using the methods of Rozovskii (1957), Kawai and Ashida (1981), or Hussein and Smith (1986). Once in motion, the particle follows a direction at an angle β from the downward direction (projection of a vertical on the embankment plane).

Stability against rotation of a particle determines incipient motion when the equilibrium of moments about the point of rotation 0 is satisfied. For instance, for the case shown in Figure 1 Section A-A, one obtains

$$l_2 F_S a_\theta = l_1 F_S \sqrt{1 - a_\theta^2} \cos\beta + l_3 F_D \cos\delta + l_4 F_L \tag{1}$$

The angle δ is measured between the streamline and the particle direction. The angles δ and β, and the moment arms l_1, l_2, l_3, l_4 are shown in Figure 1.

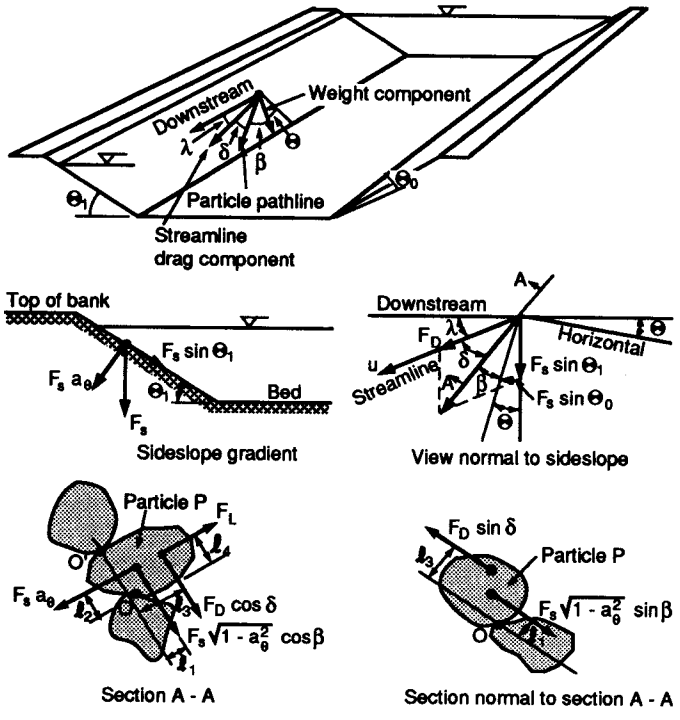

Fig. 1. Particle stability analysis.

A stability factor *SF* describing rotation about point 0 is defined as the ratio of the sum of resisting counterclockwise moments to the sum of clockwise moments generating motion. For the usual case shown in Figure 1,

$$SF = \frac{l_2 F_S a_\theta}{l_1 F_S \sqrt{1 - a_\theta^2} \cos\beta + l_3 F_D \cos\delta + l_4 F_L} \tag{2}$$

Notice that equilibrium about point 0′ also deserves consideration in some cases.
Because the stability factor *SF* equals unity when the angle θ_0 or θ_1 equals the angle of repose ϕ under static fluid conditions ($F_D = F_L = 0$), it is found that $\tan\phi = l_2/l_1$. Dividing both the numerator and the denominator by $l_1 F_S$, transforms Equation 2 into:

$$SF = \frac{a_\theta \tan\phi}{\eta_1 \tan\phi + \sqrt{1 - a_\theta^2} \cos\beta} \tag{3}$$

given,

$$\eta_1 = M + N\cos\delta \tag{4}$$

in which,

$$M = \frac{l_4 F_L}{l_2 F_S}; \qquad \text{and} \qquad N = \frac{l_3 F_D}{l_2 F_S}.$$

The variable η_1 is called the stability number for the particle on the side slope. The variable η_1 relates to the stability number $\eta_0 = M + N$ for particles on a plane horizontal surface $\theta_0 = \theta_1 = \delta = 0$ after considering $\lambda + \delta + \beta + \theta = 90°$:

$$\eta_1 = \eta_0 \left\{ \frac{(M/N) + \sin(\lambda + \beta + \theta)}{1 + (M/N)} \right\} \tag{5}$$

For flow on a plane horizontal surface, the particle stability number 0 simply corresponds to

$$\eta_0 = \frac{\tau_0}{\tau_c} \tag{6}$$

This parameter η_0 represents a normalized form of the Shields parameter. Incipient motion of particles on a plane bed under turbulent flow over hydraulically rough boundaries corresponds to $\eta_0 = 1$ when $\tau_c \simeq 0.047(G-1)\rho d_{50}$ where G is the particle specific gravity, d_{50} is the median grain diameter, is the mass density of the fluid, and g is the gravitation acceleration.
The second equilibrium condition given by the direction of the particle along the section normal to A-A in Figure 1 is:

$$l_3 F_D \sin\delta = l_1 F_S \sqrt{1 - a_\theta^2} \sin\beta \tag{7}$$

Writing δ as a function of λ, θ and β, and solving for β gives

$$\beta = \tan^{-1}\left\{ \frac{\cos(\lambda + \theta)}{\dfrac{(M+N)\sqrt{1 - a_\theta^2}}{N\eta_0 \tan\phi} + \sin(\lambda + \theta)} \right\} \tag{8}$$

In summary, the stability factors for particles on side slopes can be calculated from Equation 3 after solving successively Equations 6, 8 and 5, with the use of two geometric relationships, $a_\theta = \sqrt{\cos^2\theta_1 - \sin^2\theta_0}$ and $\tan\theta = \sin\theta_0/\sin\theta_1$. Information on lift-drag ratios can be found in Ikeda (1974) and Patnaik et al. (1994). For practical application, one can use $M = N$ because the calculations of stability factor is not very sensitive to the M/N ratio. A particle is stable (immobile) when $SF > 1$ and is unstable (mobile) when $SF < 1$. Impending motion corresponds to $SF = 1$. This method for SF reduces to Stevens and Simons (1971) when $\theta_0 = 0$. The deflection angle of a moving particle $\lambda_s = \pi/2 - \beta - \theta$ is defined with respect to the downstream direction with β calculated from Equation 8.

2.2 *Application*

The applicability of this method to particle motion on a point bar is illustrated with the following parametric analysis of the particle direction angle λ_s and the stability factor *SF*. Consider a flume at a downstream slope $\theta_0 = 0.19°$ and a particle on a point bar at a side slope angle $\theta_1 = 32°$. Assume flow conditions such that a coarse sand particle corresponds $\eta_0 = 4.5$ and a fine sand particle corresponds to $\eta_0 = 18$. It will be shown in Section 3 that these values correspond to the experimental conditions, respectively for coarse sand ($\eta_0 = 4.5$) and fine sand ($\eta_0 = 18$). The parametric variability of the streamline deviation angle λ on the point bar is examined within the range of upslope angles from –5° to –30°. Figure 2 shows the particle deflection angle λ_s calculated for both sand sizes. The solid line represents coarse sand at $\eta_0 = 4.5$ and the dashed line applied to fine sand at $\eta_0 = 18.0$. It is found that the particle direction angle λ_s decreases as the streamline angle $|\lambda|$ increases. At small streamline deviation angles, coarse particles roll down the point bar and move toward the thalweg. Fine sand particles ($\eta_0 = 18.0$) move up the point bar toward the inner bank of the channel bend.

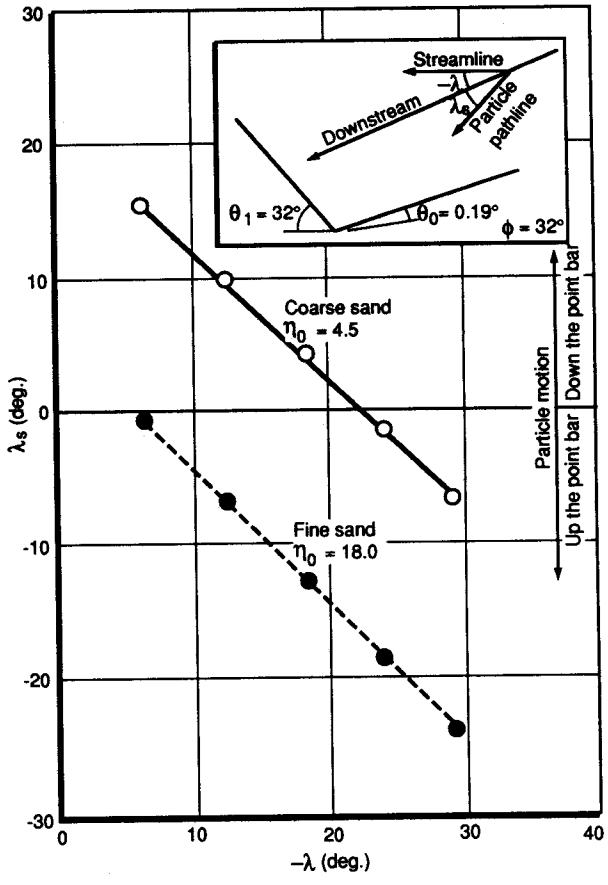

Fig. 2. Relation between λ_s and λ ($M/N = 1$).

The stability factor of a particle located on the point bar is then discussed. Figure 3 shows the relation between the calculated particle stability factor *SF* and the dimensionless sideslope angle θ_1/ϕ, where ϕ is the angle of repose. Curves for four values of streamline deviation angle are λ shown.

Notice that in meandering channels the deviation angle λ is acting toward the thalweg near the outer bank and λ is negative or applied toward the point bar near the inner bank. The upper figure represents the case of coarse sand at $\eta_0 = 4.5$ and the lower figure describes the case of fine sand at $\eta_0 = 18.0$. In both figures, the horizontal dotted lines indicate the equilibrium stability factor SF_* corresponding to the case of a flat bed ($\theta_1 = 0$) in a straight channel ($\lambda = 0$). The right-hand side of $\theta_1/\phi = 0(\lambda > 0)$ indicates the outer bank and the left-hand side of $\theta_1/\phi = 0(\lambda > 0)$ indicates the point bar.

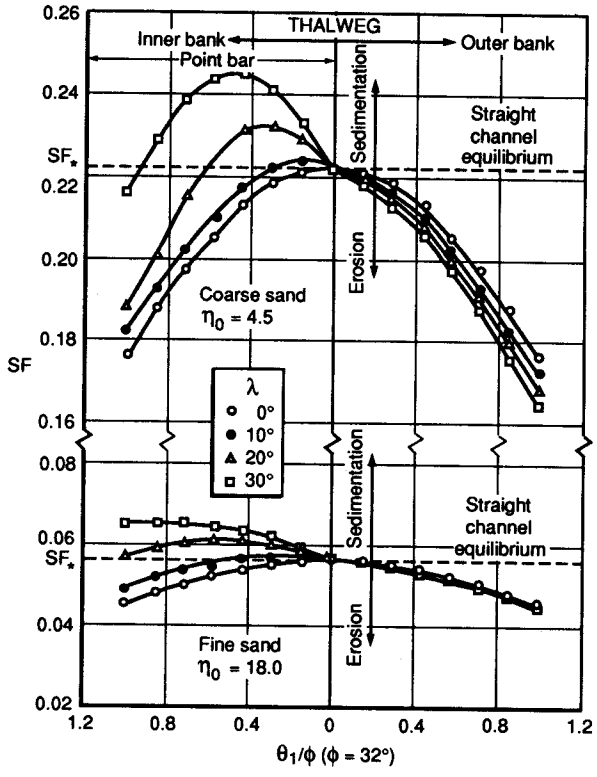

Fig. 3. Relation between SF and θ_1/ϕ ($M/N = 1$).

Relative to the equilibrium condition in a straight flat bed channel erosion occurs where $SF < SF_*$ and sedimentation occurs where $SF > SF_*$. In the positive range of λ (the outer bank) SF decreases according to the increase in λ and θ_1/ϕ, and the calculated results indicate that when compared with a straight channel, the scour is to be expected near the outer bank of meandering channels. On the point bar, particle stability depends on the upslope streamline deviation angle $|\lambda|$ and the relative side slope angle θ_1/ϕ. In the range in which θ_1/ϕ is small and $|\lambda|$ is large, the tendency of the deposition is due to $SF > SF_*$. At point bar side slopes θ_1 approaching the angle of repose ϕ, a large upslope streamline deviation angle $|\lambda|$ is required to prevent scour and induce settling. When comparing the case of coarse sand at $\eta_0 = 4.5$ and the case of fine sand at $\eta_0 = 18.0$ at steep side slope angles $\theta_1/\phi > 0.8$, the deposition of fine sands is possible when $|\lambda| > 18°$. Conversely, point bars with coarse sand at $\eta_0 = 4.5$ maintain a strong tendency to scour as θ_1 approaches ϕ unless $|\lambda| > 30°$. Although both fine and coarse sands deposit on flat point bars, only fine sand is likely to deposit on fairly steep point bars.

The difference between the shape of the various *SF* curves on steep point bars (left-hand side of Fig. 3) for coarse and fine sands is expected to play a role in the morphological extent of point bars in sharp meander bends. For instance, from Figure 3 with $|\lambda| = 20°$, one would expect settling of fine sand on steep point bars $\theta_l/\phi > 0.8$, where coarse sands would be eroded. This effect combined with the results of Figure 2 showing that coarse sands move toward the thalweg indicate that the extent of point bar deposits would be larger for fine sands than coarse sands given identical flow conditions.

The results of this theoretical analysis deserve experimental testing to determine whether or not fine sand point bars have a larger extent than coarse sand point bars under identical flow conditions.

3 Laboratory experiments

Laboratory experiments were carried out in the curved outdoor flume at Maizuru College of Technology, Kyoto, Japan. The objective of the experiment was to examine whether or not fine sand point bars have a larger extent than coarse sand given identical flow conditions. The result of this experiment serves to test the previously detailed particle stability analysis. Two cases of point bar deposits in narrow sharp bends are described: 1) 0.6 mm coarse sand; and 2) 0.15 mm fine sand. The essence of the experiment is the following. In Run 1, given a constant supply of coarse sands in a 90° bend, a point bar forms under steady flow conditions. Once equilibrium is reached, the coarse-grained point bar is fixed and the constant supply of sediment is changed from coarse sand to fine sand in Run 2 until a new point bar deposit reaches equilibrium. The results between the extent of coarse versus fine-grained point bars are then discussed.

3.1 *Experimental procedure*

The experimental study is carried out in a curved flume with fixed vertical sidewalls. The dimensions sketched in Figure 4 include a 0.2 m width, 90° bend angle, 0.6 m centerline bend radius, and two straight sections (4.5 m and 1.6 m upstream and downstream 1.6 m). The hydraulic conditions are listed in Table 1. Uniform coarse sand with a mean diameter of 0.6 mm is used in Run 1, and fine sand with a mean diameter of 0.15 mm is used in Run 2.

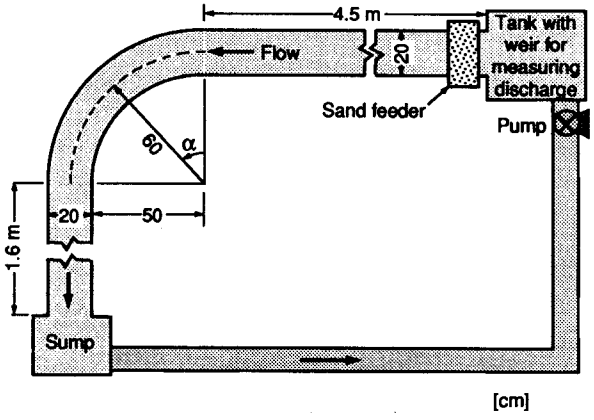

Fig. 4. Sketch of experimental flume.

Table 1. Experimental conditions at the upstream reach.

	Sand size d_s (mm)	Discharge Q (ℓ/s)	Upstream bed slope	Upstream flow depth h (cm)	Shear velocity u_* (m/s)	Shields parameter τ_*	Froude number
Run 1	0.6	4.0	1/300	4.1	0.037	0.14	0.77
Run 2	0.15	4.0	1/330	4.3	0.036	0.54	0.71

Initially, the flume bed is set transversely flat ($\theta_1 = 0$) with a longitudinal slope 1/300 ($\theta_0 = 0.19°$). Run 1 involves a steady flow of water ($Q = 4.0$ *l/s*) and a constant upstream supply of coarse sand at a rate of $Q_B = 1.44$ cm^3/s. The sediment discharge at the downstream end of the flume is measured at five minute intervals. These measurements in Figure 5 indicate that equilibrium is reached after a period of about 200 minutes. When the outgoing sediment discharge equals the supplied sediment discharge at 1.44 cm^3/s, the bed profile reaches equilibrium conditions and does not change with time. After equilibrium is achieved, the water surface profile and the bed profile are measured using point gauges. The equilibrium bed and water surface profiles for Run 1 are shown in Figure 6. The flume bed profile is then fixed using mortar. After the fixed bed profile was measured, Run 2 begins with the same water discharge (Q = 4.0 *l/s*) under a constant supply of fine sand at a sediment concentration C = 900 mg/*l*. Since fine sands move both in suspension and as bed load, it becomes more difficult to accurately measure the downstream sediment discharge. Instead of comparing incoming and outgoing sediment discharges, the bed elevation is monitored and the experiment lasts a sufficiently long period of time for the bed elevation to remain unchanged. The state when bed elevation does not change over a long period of time is referred to as quasi-equilibrium. The profiles of water surface and flume bed deviations are measured at quasi-equilibrium. The results for fine sand in Run 2 are shown in Figure 7 for comparison with the coarse-sand point bars from Run 1 in Figure 6.

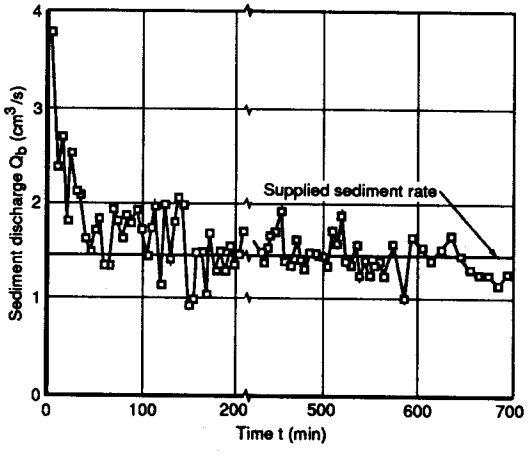

Fig. 5. Sediment discharge measured at the downstream end of the flume.

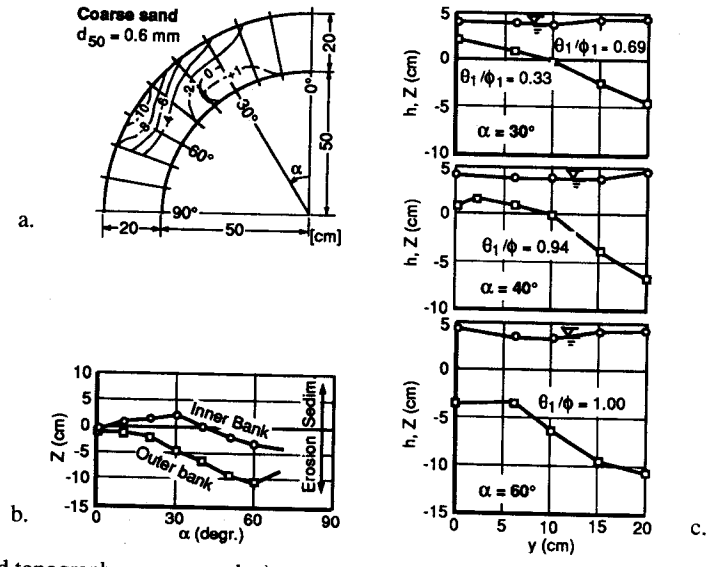

Fig. 6. Bed topography coarse sand: a) topography; b) longitudinal profile; and c) cross-sections.

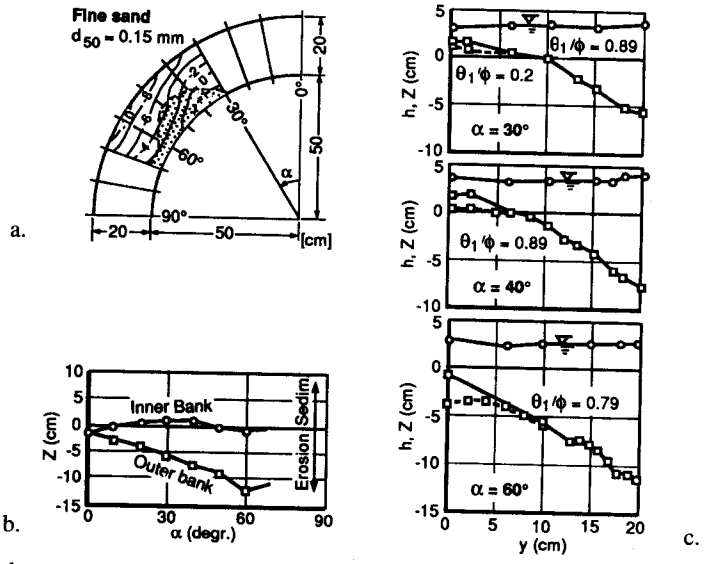

Fig. 7. Bed topography for fine sand: a) topography; b) longitudinal profile; c) cross-sections.

3.2 *Experimental results*

Figure 6 shows the equilibrium bed topography and longitudinal profiles in the curved section of the flume in the case of coarse sand. Figure 6a shows the bed topography, with a zero reference to the initial bed level, a positive elevation indicates net sedimentation in cm, and a negative elevation indicates net erosion of the bed in cm. Figure 6b shows the longitudinal bed profiles along the inner and outer banks. The corresponding cross-sectional profiles are shown on Figure 6c.

As expected, bed scour is observed near the outer bank. The maximum depth of scour reached 11.0 cm at near bend angle $\alpha = 60°$. Near the inner bank, both deposition and scour occurred along the bend. At bend angles $0° < \alpha < 40°$, a point bar was formed near the inner bank from the deposit of coarse sand above the initial bed level. Unexpectedly, farther downstream at $\alpha > 40°$ the point bar did not form and the coarse sand bed experienced scour from the initial bed level. The side slope angles θ_1 were respectively 24°, 31° and 35° at the bend angles $\alpha = 30°$, 40° and 60°. In two cases, the side slope angles are comparable to the angle of repose of the bed material.

Several observations confirm those of previous studies, such as the deviation of streamline direction near the bed from the outer bank toward the inner bank due to secondary current in a bend. Consequently, bed scour reaches the outer bank while bed material should deposit near the inner bank to form a point bar. The maximum scour depth is observed at a bend angle $\alpha = 60°$ near the outer bank. In this experiment, the bed deformation near the outer bank and the inner bank from bend angle $0° < \alpha < 40°$ is similar to previous studies. However, the bed deformation when $\alpha > 40°$ is different from previous studies.

The results of Run 2, with fine sand are shown in Figure 7a in terms of changes in bed topography with a zero reference to the initial bed level, a positive sedimentation is indicated in cm, negative values indicate erosion in cm. Figure 7b shows the longitudinal bed profiles along the inner and the outer banks, with the corresponding cross-sectional profiles in Figure 7c. In Figure 7c the broken lines indicate the bed elevation for coarse sand fixed with mortar. The upper solid line indicates the accumulation of fine sand on the point bar.

Fine sand deposits on the point bar at angles $\alpha > 40°$. The fine sand deposit near the inner bank fills the area which has been previously scoured with coarse sand in Run 1. The maximum thickness of fine sand deposit reaches 4 cm and the bed level at the inner bank corresponds closely to the initial bed level.

4 Discussion

One may appropriately ask: why did fine sand particles deposit where coarse particles were eroded under the same flow conditions? These observations demonstrate that point bar deposits depend on particle size. The point bar deposits where $\alpha > 40°$ are different for coarse sand (Run 1) and fine sand (Run 2). These results support the calculations shown in Figure 2 that coarse sand particles move toward the outer bank where $\alpha > 40°$, while fine sand particles move toward the inner bank. These path directions depend on the balance between the upslope moment (UM) induced by the secondary current and the downslope gravitational moment (DM). Near-bed sand particles move downslope for coarse sands along the bed because UM < DM in Run 1 and move upslope for fine sands because UM > DM in Run 2. The difference in path direction angle between coarse and fine sands results in different point bar configurations.

In these experiments, the normalized Shields parameter is $\eta_0 = 4.5$ for coarse sand ($d_s = 0.6$ mm) was and is $\eta_0 = 18.0$ for fine sand. Therefore, the calculated results of the deflection angle of sand particle λ_s correspond to those of Figure 2. Values of η_0 were calculated using the mean flow depth and average energy slope in the bend. As readily explained, this figure shows that the coarse sand particles move from the inner bank toward the outer bank and the fine sand particles move from the outer bank toward the inner bank. The angle at which particles move is extremely important to determine the extent of point bars. It is unlikely that point bars would form if bedload particles were deflected toward the thalweg of meandering streams.

The morphology of point bars in sinuous channels seems closely linked to the particle direction angle λ_s, or β, here calculated from the three-dimensional particle stability analysis. Point bars can have a large extent when the angle $\beta > 90°$, i.e. for particles sufficiently small for the upslope drag force moment UM to be dominant compared to the downslope weight moment DM. Conversely, particles sufficiently coarse for DM > UM, move toward the thalweg despite favorable secondary circulation and coarse-grained point bars tend to be much smaller than their fine-grained counterparts.

Figure 8 shows the particle stability diagram for coarse and fine sands given the measured range of θ_l/ϕ within the range $-20° < \lambda < -10°$, the stability factor *SF* for coarse sand (upper figure) is smaller than SF_* ($\lambda = 0$ and $\theta_l = 0$), when $\theta_l/\phi > 0.6$. Point bar steepening in coarse sand will thus result in erosion of the point bar. Conversely, point bars of fine sand (the lower figure) are more or less in equilibrium between erosion and deposition regardless of the side slope angle θ_l/ϕ.

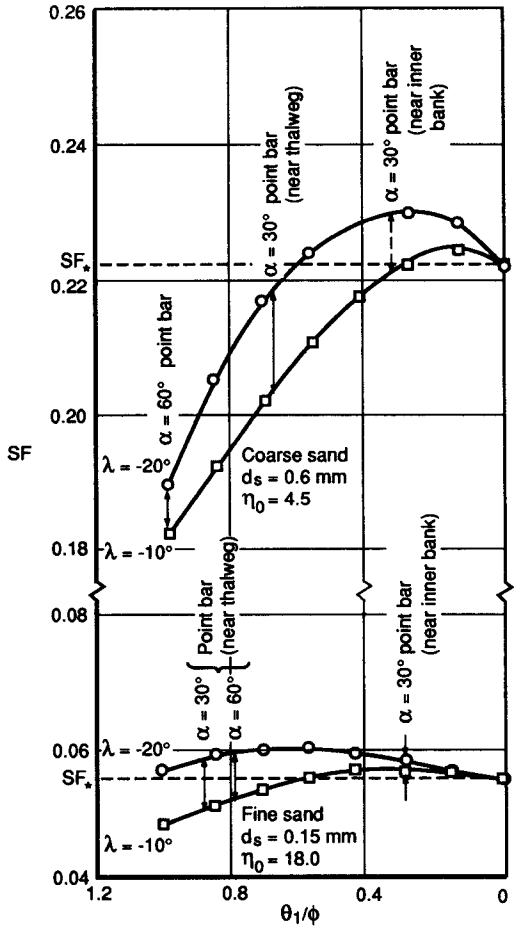

Fig. 8. Particle stability for the experimental conditions.

More specifically, the experimental values of θ_l/ϕ are illustrated on Figure 8 at two cross-sections, $\alpha = 30°$ and $\alpha = 60°$ respectively. In the case of coarse sand in the upper figure, at $\alpha = 30°$, the near thalweg portion of the point bar is degrading while the portion near the inner bank is aggrading.

Farther downstream, at $\alpha = 60°$, point bar scour has occurred over most of the channel width as calculated on Figure 8. The case of fine sand under similar hydraulic conditions is strikingly different, sedimentation occurs at angles $\theta_1/\phi = 0.6$. Consequently, at $\alpha = 30°$, the near-thalweg portion of the point bar is essentially stable, depending on the streamline deviation angle λ, while the point bar slightly aggrades near the inner bank. Farther downstream at $\alpha = 60°$, the point bar is in near equilibrium along its entire cross-section. Overall, the experimental observations are correctly predicted by the particle stability diagram in Figure 8.

This analysis highlights that physical models of meandering channels require careful consideration of two factors: 1) adequate selection of particle size and density; and 2) effects of distortion on point-bar geometry. First, particle size and density determine the magnitude of the drag force and the weight component. These two components determine the orientation angle λ_s, or β, of the particle. In order to preserve similitude in the formation of point bars in the physical model, like the prototype, the particle direction angle should be essentially the same in both cases. This means that once the density of the material has been determined, the particle size can be calculated to give the same angle β from Equation 8.

The effects of distortion are also important in that the vertical scale is often exaggerated for hydrodynamic reasons. It is important to consider that vertical distortion also implies steepening of the point bar. In some cases, like in this experiment, the point bar side-slope angle becomes very close to the angle of repose of the transported sediment with particle stability being smaller on steep side slopes, high distortion tends to form smaller point bars than would be expected for the prototype.

5 Conclusions

Bed deformation in a bend was discussed theoretically and experimentally with our attention focused on point bar formation and possible scour near the inner bank in the case of coarse-grained point bars. Previous studies had shown that the deposition occurs near the inner bank in bends. However, this experiment shows that scour is also possible near the inner bank when the bed material is coarse. The point bar formation experiment in which the supply of coarse sand is replaced with a supply of fine sand indicates that the point bar configuration depends on particle size. Fine sand point bars are larger than coarse sand counterparts. Under identical hydraulic conditions the effect is more pronounced in narrow sharp bends.

A three-dimensional particle stability analysis can be used to examine the extent of point bars. The balance between the upslope moment induced by the secondary current and the downslope gravitational moment both acting on the bed particles plays a dominant role. Calculations of the stability factor *SF* and the particle direction angle β or λ_s become very important. The theoretical approach to the stability of the bank in a bend corresponds to experimental observations. The calculated results correctly predict that erosion occurs when using coarse sand and that sedimentation occurs when using fine sands, thus resulting in different point bar configurations under identical flow conditions.

Acknowledgements

The authors express their gratitude to Masanori Michiue, Dean of Technology of Tottori University in Japan, for his useful advice regarding the experiments in this paper. This study was completed during the first author's sabbatical research at Colorado State University.

Notations

a_θ	$\sqrt{\cos^2\theta_1 - \sin^2\theta_0}$
C	sediment concentration
d_s	particle diameter
F_B	buoyancy force
F_D	drag force
F_L	lift force
F_S	submerged weight of particle
F_W	particle weight
g	gravitational acceleration
G	specific gravity of the sediment particle
l_1, l_2, l_3, l_4	moment arms
M	ratio of lift to submerged weight moments
N	ratio of drag to submerged weight moments
Q	water discharge
Q_B	sediment discharge
SF	particle stability factor
SF_*	equilibrium stability factor
α	bend angle
β	particle direction angle with respect to maximum descent
δ	angle between streamline and particle directions
η_0	plane bed stability number
η_1	side slope stability number
θ	direction of steepest descent
θ_0	downstream bed slope angle
θ_1	side slope angle
λ	angle between streamline and downstream directions
λ_s	particle direction angle with respect to downstream direction
τ_0	applied bed shear stress
τ_c	critical plane bed shear stress
ρ	mass density of the fluid
ϕ	bed material angle of repose

7 References

ELLIOTT, C.M. editor, 1984, "River Meandering," Proc., Conference on Rivers '83, New Orleans, LA, ASCE, NY, 1036 p.

HUSSEIN, K. and SMITH, V.H., 1986, "Flow and Bed Deviation Angle in Curved Open Channels," J. Hydr. Research, IAHR, 24(2), pp. 93–108.

IKEDA, S., 1974, "On Secondary Flow and Dynamic Equilibrium of Transverse Bed Profile in Alluvial Curved Open Channel," Proc. of JSCE, No. 229, Sept., pp. 55–65, (Japanese).

IKEDA, S., 1982, "Lateral Bed Load Transport on Side Slopes," J. Hydr. Div., ASCE, 108(HY11), pp. 1369–1373.

IKEDA, S. and PARKER, G. editors, 1989, "River Meandering," Water Resources Monograph, AGU, Washington, D.C., 485 p.

JULIEN, P.Y., 1995, "Erosion and Sedimentation," Cambridge University Press, NY, 280 p.

KAWAI, S. and ASHIDA, K., 1981, "Experimental Study on the Dividing Ratios of Water and Sediment at Junction in Open Channels," Proc. 25th Japanese Conf. in Hydraulics (Japanese).

KIKKAWA, H., IKEDA, S. and KITAGAWA, A., 1976, "Flow and Bed Topography in Curved Open Channels," J. Hydr. Div., ASCE, 102(HY9), pp. 1327–1342.

KOCH, F.G. and FLOKSTRA, C., 1980, "Bed Level Computations for Curved Alluvial Channels," Proc. of the XIX Congress of the IAHR, 2, New Delhi, India, 357 p.

MURAMOTO, Y., SAKAMOTO, T. and YOSHIMURA, T., 1968, "Studies on Sedimentation in Curved Open-channels", Disaster Prevention Research Inst. Annuals No. 11B, Kyoto University, pp. 291–310 (Japanese).

ODGAARD, A.J., 1981, "Transverse Bed Slope in Alluvial Channel Bends," J. Hydr. Div., ASCE, 107(HY12), pp. 1677–1694.

PARKER, G., 1984, "Discussion of Lateral Bed Load Transport on Side Slopes," J. Hydr. Div., ASCE, 110(HY2), pp. 197–203.

PATNAIK, P.C., VITTAL, N. and PANDE, P.K., 1994, "Lift Coefficient of a Stationary Sphere in Gradient Flow," J. Hydr. Research, IAHR, Vol. 32, No. 3, pp. 471–480.

ROZOVSKII, I.L., 1957, "Flow of Water in Bends of Open Channel," Acad. Sciences of the USSR.

SHEN, H.W., editor, 1990, "Movable Bed Physical Models," NATO ASI Series, Kluwer Acad. Pub., 171 p.

STEVENS, M.A. and SIMONS, D.B., 1971, "Stability Analysis for Coarse Granular Material on Slopes," Chap. 17 in River Mechanics, Water Res. Publ., Littleton, Colorado.

STRUIKSMA, N., K.W. OLESEN, C. FLOKSTRA and H.J. DE VRIEND, 1985. "Bed Deformation in Alluvial Channel Bends," J. Hydr. Res., IAHR, 23(1), pp. 57–79.

TALMON, A.M., N. STRUIKSMA and M.C.L.M. VAN MIERLO, 1995, "Laboratory Measurements of the Direction of Sediment Transport on Transverse Alluvial-Bed Slopes," J. Hydr. Res., IAHR, 33(4), pp. 495–517.

YEN, C.L., 1970, "Bed Topography Effect on Flow in a Meander," J. Hydr. Div., ASCE, 96(HY1), pp. 57–73.

ZIMMERMANN, C. and J.F. KENNEDY, 1978, "Transverse Bed Slope in Curved Alluvial Streams," J. Hydr. Div., ASCE, 104(HY1), pp. 33–48.